nature neuroscience

ARTICLES

RIM1 confers sustained activity and neurotransmitter vesicle anchoring to presynaptic Ca^{2+} channels

Shigeki Kiyonaka[1], Minoru Wakamori[1], Takafumi Miki[1], Yoshitsugu Uriu[1], Mio Nonaka[2], Haruhiko Bito[2], Aaron M Beedle[3], Emiko Mori[1], Yuji Hara[1,3], Michel De Waard[4], Motoi Kanagawa[3], Makoto Itakura[5], Masami Takahashi[5], Kevin P Campbell[3] & Yasuo Mori[1]

The molecular organization of presynaptic active zones is important for the neurotransmitter release that is triggered by depolarization-induced Ca^{2+} influx. Here, we demonstrate a previously unknown interaction between two components of the presynaptic active zone, RIM1 and voltage-dependent Ca^{2+} channels (VDCCs), that controls neurotransmitter release in mammalian neurons. RIM1 associated with VDCC β-subunits via its C terminus to markedly suppress voltage-dependent inactivation among different neuronal VDCCs. Consistently, in pheochromocytoma neuroendocrine PC12 cells, acetylcholine release was significantly potentiated by the full-length and C-terminal RIM1 constructs, but membrane docking of vesicles was enhanced only by the full-length RIM1. The β construct beta-AID dominant negative, which disrupts the RIM1-β association, accelerated the inactivation of native VDCC currents, suppressed vesicle docking and acetylcholine release in PC12 cells, and inhibited glutamate release in cultured cerebellar neurons. Thus, RIM1 association with β in the presynaptic active zone supports release via two distinct mechanisms: sustaining Ca^{2+} influx through inhibition of channel inactivation, and anchoring neurotransmitter-containing vesicles in the vicinity of VDCCs.

The presynaptic active zone is the specific site for impulse-evoked exocytosis of neurotransmitters at synapses of the nervous system in a wide variety of species[1,2]. Fine regulation of presynaptic active zone neurotransmitter release is integral to nervous system adaptive functions, including learning, memory and cognition. The molecular organization of presynaptic active zones, where synaptic vesicles are docked in close vicinity to VDCCs at the presynaptic membrane, is essential for controlling the neurotransmitter release triggered by depolarization-induced Ca^{2+} influx. The spacing between VDCCs and vesicles influences the dynamic properties of synaptic transmission[3]. However, the molecular determinants that maintain vesicles and VDCCs within a physiologically appropriate distance have remained elusive.

Originally identified as a putative effector for the synaptic vesicle protein Rab3 (ref. 4), RIM1 is part of the RIM superfamily, whose members share a common C_2B domain at their C termini[5]. RIM1 interacts with other presynaptic active zone protein components, including Munc13, ELKS (also known as CAST), RIM-BP and liprins, to form a protein scaffold in the presynaptic nerve terminal[6–10]. Mouse knockouts showed that, in different types of synapses, RIM1 is essential for different forms of synaptic plasticity[9,11]. In the CA1-region Schaffer-collateral excitatory synapses and GABAergic synapses, RIM1 maintains normal neurotransmitter release and short-term synaptic plasticity. In excitatory CA3-region mossy fiber synapses and cerebellar parallel fiber synapses, RIM1 is necessary for presynaptic long-term synaptic plasticity. In autapses, the RIM1 deletion significantly reduces the readily releasable pool of vesicles, and it alters short-term plasticity and the properties of evoked asynchronous release[12]. However, in spite of this progress in understanding RIM1 functions, the mechanisms by which RIM1 acts remain unknown. Moreover, the physiological functions of other RIM isoforms (RIM2, RIM3 and RIM4)[5] remain unclear.

Multiple types of VDCCs that are distinguished on the basis of biophysical and pharmacological properties coexist in neurons[13]. High voltage–activated types of VDCCs that are essential for neurotransmitter release include N-, P/Q-, R- and L-types[14–16]. VDCCs are heteromultimeric protein complexes composed of the pore-forming α_1, designated as Ca_v, and auxiliary subunits α_2/δ, β and γ[17]. The α_1 subunit is encoded by ten distinct genes, whose correspondence with functional types is largely elucidated[13,17]. VDCC complexes are associated, primarily via interactions with the α_1 subunit[18–25], with presynaptic and postsynaptic proteins including syntaxin, SNAP-25, synaptotagmin, CASK and Mint. The α_1 and β subunits interact to enhance functional channel trafficking to the plasma membrane[26,27]

[1]Department of Synthetic Chemistry and Biological Chemistry, Graduate School of Engineering, Kyoto University, Katsura Campus, Nishikyo-ku, Kyoto 615-8510, Japan. [2]Department of Neurochemistry, University of Tokyo Graduate School of Medicine, Hongo 7-3-1, Bunkyo-ku, Tokyo 113-0033, Japan. [3]Howard Hughes Medical Institute and Departments of Physiology and Biophysics, Internal Medicine, and Neurology, University of Iowa Roy J. and Lucille A. Carver College of Medicine, 285 Newton Road, Iowa City, Iowa 52242-1101, USA. [4]Inserm U607, Laboratoire Canaux Calciques, Fonctions et Pathologies, 17 Rue des Martyrs, Bâtiment C3, 38054 Grenoble Cedex 09, France. [5]Department of Biochemistry, Kitasato University School of Medicine, Kitasato 1-15-1, Sagamihara, Kanagawa 228-8555, Japan. Correspondence should be addressed to Y.M. (mori@sbchem.kyoto-u.ac.jp).

Received 23 February; accepted 2 April; published online 13 May 2007; doi:10.1038/nn1904

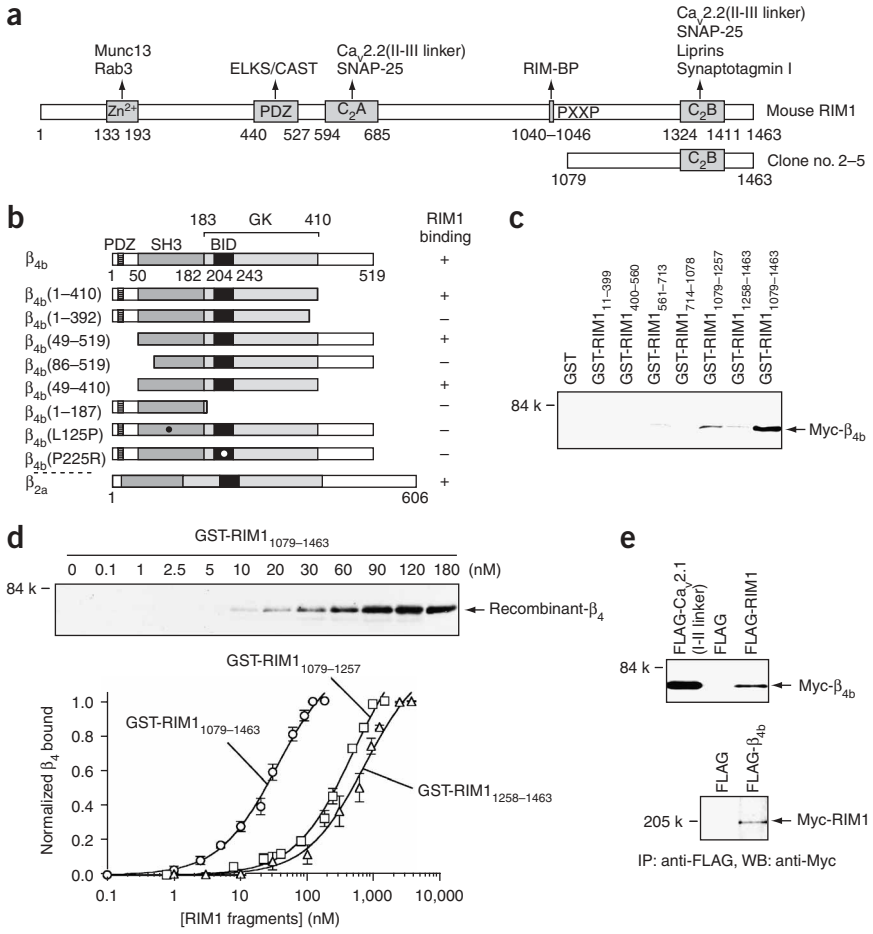

Figure 1 Direct interaction of RIM1 with the VDCC β_{4b} subunit. (**a**) Domain structure of mouse RIM1. Arrows indicate molecules interacting with RIM1 at the Zn^{2+}-finger–like domain (Zn^{2+}), PDZ domain (PDZ), first and second C_2 domains (C_2A and C_2B) and proline-rich region (PXXP)[4,6–10]. The protein region encoded by clone no. 2–5 is also indicated. (**b**) Mapping of RIM1-binding sites on β_{4b} by the yeast two-hybrid assay. β-subunit constructs in bait vectors were tested with RIM1 in the prey vector. The interactions were scored by β-galactosidase activity and His^+ prototrophy. (**c**) Pulldown assay of β_{4b} with GST fusion RIM1 mutants. GST fusion proteins immobilized on glutathione-Sepharose beads were incubated with cell lysates obtained from Myc-β_{4b}–transfected HEK293 cells. Bound proteins were analyzed by western blotting (WB) using antibody for Myc. (**d**) *In vitro* association between the purified GST-RIM1 fusion constructs and recombinant β_4 subunit (residues 47–475). GST-RIM1 proteins at various concentrations, incubated with β_4 (50 pM), were captured by glutathione-Sepharose beads. Captured β_4 proteins were examined by WB. The bottom panel shows the quantitative densitometric analysis of bands shown in the upper panel and in **Supplementary Figure 2**. The saturation curves were subjected to the nonlinear least-squares curve-fitting method to evaluate the apparent dissociation constant (K_d). k, kDa. (**e**) Interaction of recombinant β_{4b} and RIM1 in HEK293 cells. The interaction is evaluated by immunoprecipitation (IP) with antibody for FLAG, followed by WB with antibody for Myc. Top, physical association of Myc-β_{4b} with FLAG-RIM1 in comparison with a positive control FLAG-Ca$_v$2.1(I-II linker). Bottom, physical association of FLAG-β_{4b} with Myc-RIM1.

and to modify multiple kinetic properties[28]; the β subunit also interacts with other proteins[29–31]. Therefore, it is intriguing to investigate whether β subunits are involved in targeting VDCC complexes to specific subcellular machinery at presynaptic active zones for neurotransmitter release through as yet unidentified interactions. Here, we demonstrate a previously unknown molecular interaction between RIM1 and VDCC β subunits, both of which are essential presynaptic active zone proteins. The RIM1-β interaction supports the function of RIM1 in neurotransmitter release via two distinct mechanisms: the anchoring of neurotransmitter-containing vesicles in the vicinity of VDCCs, and the sustenance of Ca^{2+} influx through the inhibition of voltage-dependent inactivation.

RESULTS

VDCC β subunits directly interact with RIM1

To identify β subunit–interacting proteins that regulate presynaptic active zone organization, we performed yeast two-hybrid screening with a mouse brain complementary DNA library using the full-length rat β_{4b} subunit as a bait. The β_4 subunit was chosen because spontaneous β_4 mutant *Cacnb4*^{lh} (lethargic) mice[32] have clear neurological defects suggesting that β_4-containing VDCCs are physiologically significant in the brain. Screening identified a clone (no. 2-5) encoding the C-terminal region (residues 1079–1463) of the mouse RIM1 protein[4] including the C_2B domain (**Fig. 1a**). Subsequent two-hybrid assays using β_{4b} mutants showed that residues 49–410, containing major structural motifs such as the Src homology 3 (SH3) domain, the α_1-interacting domain known as BID and the guanylate kinase (GK) domain, were required for the interaction of β_{4b} with the RIM1 C terminus (**Fig. 1b**). β_{2a} also showed RIM1 interaction. *In vitro* pulldown assays using glutathione-*S*-transferase (GST) fusion constructs identified the RIM1 C terminus (residues 1079–1463) as a major β_4-interaction domain likely formed in concert by two adjacent subdomains (1079–1257 and 1258–1463; **Fig. 1c** and **Supplementary Fig. 1** online). An *in vitro* binding assay using purified β_4 and RIM1 recombinants revealed a dissociation constant (K_d) of 35.1 nM for $RIM1_{1079–1463}$, which was substantially lower than those of $RIM1_{1079–1257}$ (481 nM) and $RIM1_{1258–1463}$ (717 nM) (**Fig. 1d** and **Supplementary Fig. 2** online). These results, as well as the successful coimmunoprecipitation of full-length RIM1 with β_{4b} (**Fig. 1e**), suggest that a direct protein-protein interaction occurs between RIM1 and β_4.

RIM1 physically associates with native VDCCs in the brain

We characterized the association between native VDCCs and RIM1 biochemically using VDCC complexes enriched from mouse brains through microsome preparation, KCl wash, solubilization, heparin purification and sucrose density gradient fractionation[25]. Western blot analysis of sucrose gradient fractions showed cosedimentation of RIM1 with $Ca_v2.1$ and β_4 (**Fig. 2a**). Statistical analysis of cosedimentation data revealed a complete overlap of $Ca_v2.1$ and β_4, confirming that they associate in the VDCC complex (**Fig. 2b**). RIM1 sedimented in overlapping minor and major peaks: the latter completely overlapped with VDCC subunits, whereas the former did not cosediment with VDCC and is likely to represent a subset of RIM1 in a smaller,

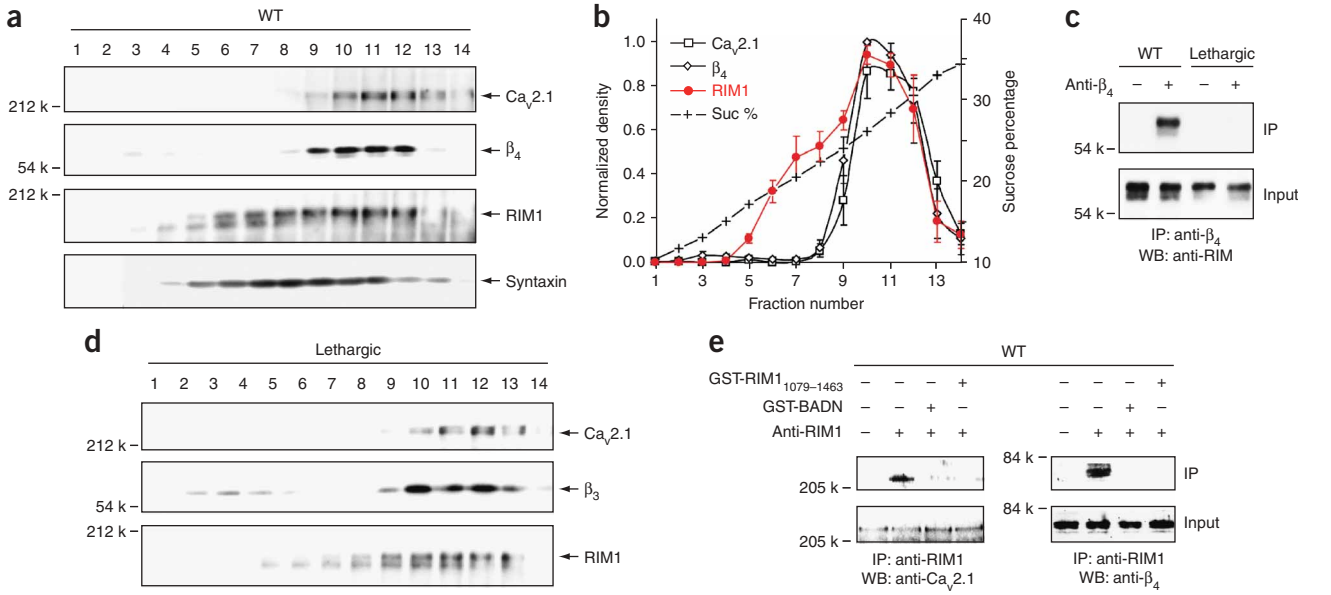

Figure 2 Association of RIM1 with native neuronal VDCC complexes. (**a**) Sucrose gradient fractionation of neuronal VDCC complexes from wild-type (WT) mouse brains and subsequent western blot (WB) showed cosedimentation of RIM1 with $Ca_v2.1$ and β_4. Syntaxin showed similar cosedimentation with RIM1. (**b**) Densitometry of $Ca_v2.1$, β_4 and RIM1 from western blots of sucrose gradient fractions. The normalized density of each protein is plotted as a function of the sucrose density fraction number. (**c**) Coimmunoprecipitation of RIM1 with the β_4 subunit. Immunoprecipitation (IP) using an antibody for β_4 and subsequent WB for RIM1 was carried out on heparin-purified samples. A preparation from lethargic mice was used as a negative control. (**d**) Sucrose gradient fractionation of neuronal VDCC complexes from lethargic mouse brains. (**e**) Coimmunoprecipitation of VDCC subunits with RIM1. The immunocomplexes were disrupted by GST-BADN or GST-$RIM1_{1079–1463}$. IP using anti-RIM1 antibody and subsequent western blotting for $Ca_v2.1$ or β_4 was carried out.

non-VDCC complex. Syntaxin, a VDCC-interacting protein[18–21], showed similar cosedimentation with RIM1. Immunoprecipitation analysis of heparin-purified samples confirmed that the cosedimentation of RIM1 is due to its specific interaction with VDCC subunits (**Fig. 2c**). Antibody specific for β_4 precipitated RIM1 from wild-type mice, but not from lethargic mice (which carry a mutated form of the gene *Cacnb4*), expressing truncated β_4 protein lacking the α_1-interacting region[32,33]. It is unlikely that the β_4 isoform exclusively mediates the RIM1-VDCC association in the brain, as wild-type and lethargic mice were indistinguishable in the sucrose gradient profile (**Fig. 2d**). We designed a dominant-negative suppressor β_{4b} fusion construct (beta-AID dominant negative, BADN) to dissociate the activity of β-binding proteins such as RIM1 from the functional VDCC complex (**Supplementary Fig. 3** online). As residues 49–410 of the entire 519-amino-acid β_{4b} sequence are required for RIM1 binding (**Fig. 1b**), BADN was designed from the 'full-length' β_{4b} to efficiently quench RIM1. BADN also carries the β-interacting AID region from $Ca_v2.1$ buried at the α_1-binding site[33]. Because the intermolecular association of BADN with VDCC α_1 is inhibited by the intramolecular occlusion of the α_1-binding site in BADN, overexpression of BADN should deprive native β subunits of RIM1 without affecting their association with α_1. *In vitro* binding and coimmunoprecipitation experiments showed that BADN could bind to RIM1, but not to the AID-containing I-II linker region of $Ca_v2.1$ (**Supplementary Fig. 3**). Notably, the native RIM1-β association in partially purified brain VDCCs was disrupted by an 8-h co-incubation with 100 nM GST fusion proteins for BADN or $RIM1_{1079–1463}$ (**Fig. 2e**). *In vitro* binding of β_4 to $RIM1_{1079–1463}$ rapidly decayed with the addition of excess BADN (200 nM), indicating that this disruption is attributable to displacement of binding partners in the native association (**Supplementary Fig. 3**). These results provide evidence for a physiological association between native RIM1 and P/Q-type VDCCs via the β subunit in brain.

RIM1 targets to VDCC via β subunits at the plasma membrane

In recombinant HEK293 cells, β_{4b} and RIM1 were concentrated at the plasma membrane when they were coexpressed with the P/Q-type $Ca_v2.1$ α_1 subunit, whereas they were diffusively colocalized throughout the intracellular area in the absence of $Ca_v2.1$ (**Fig. 3a** and **Supplementary Fig. 4** online). The ratio of the fluorescence intensity at the plasma membrane, PM, to that in the cytoplasm, CYT—F_{PM}/F_{CYT}—was 0.52 ± 0.07 and 0.48 ± 0.07 with $Ca_v2.1$ and 0.10 ± 0.02 and 0.08 ± 0.02 without $Ca_v2.1$ for β_{4b} and RIM1, respectively. RIM1 localization to the plasma membrane via a membrane-targeted β-binding domain[27] composed of CD8 and the $Ca_v2.1$ I-II linker was elicited only after β_{4b} expression (**Fig. 3b** and **Supplementary Fig. 4**). The F_{PM}/F_{CYT} ratio was 0.29 ± 0.03 and 0.27 ± 0.02 with β_{4b}, and 0.08 ± 0.01 and 0.08 ± 0.02 without β_{4b} for the $Ca_v2.1$ I-II linker and RIM1, respectively. Notably, both the $Ca_v2.1$-mediated plasma membrane colocalization of RIM1 and β_{4b}, and the β_{4b}-mediated colocalization of RIM1 and the $Ca_v2.1$ I-II linker, were disrupted by BADN. In the presence of BADN, F_{PM}/F_{CYT} was 0.56 ± 0.11 and 0.19 ± 0.04 for β_{4b} and RIM1, respectively; and F_{PM}/F_{CYT} was 0.33 ± 0.04 and 0.13 ± 0.04 for the $Ca_v2.1$ I-II linker and RIM1, respectively. Thus, the RIM1-β_{4b} interaction is likely to be essential for the assembly of RIM1 with VDCC at the plasma membrane.

In cultured hippocampal neurons, RIM1 and β_{4b} both accumulated near presynaptic termini, in parallel with $Ca_v2.1$ clustering. These events had a substantially later onset than synaptogenesis, as shown by the synapsin I clustering observed at 8 days *in vitro* (DIV, **Fig. 3c,d**). Quantitative imaging showed that overexpression of either BADN or the RIM1 C terminus, $RIM1_{1079–1463}$, impaired the $Ca_v2.1$ clustering in presynaptic varicosities (**Fig. 3e,f**). The coincident targeting of RIM1 and β_{4b}, as well as the blockade of $Ca_v2.1$ accumulation by quenching of RIM1 and βs, suggests that the RIM1-β interaction regulates the localization of VDCCs at the presynaptic membrane. Because RIM1

interacts with multiple proteins (**Fig. 1a**), the RIM1 effect observed using BADN and $RIM1_{1079–1463}$ could also be attributed to the quenching of other RIM interactions at different subcellular locations. However, a recent immunostaining study showed that the staining intensities for $Ca_v2.2$ and RIM covary at a giant calyx-type synapse[34], consistent with the idea that they are both components of transmitter release sites.

RIM1-β interaction modulates inactivation of VDCCs

To elucidate the functional significance of direct RIM1-β_4 coupling, we characterized whole-cell Ba^{2+} currents through recombinant VDCCs expressed as $\alpha_1\alpha_2/\delta\beta$ complexes containing various neuronal α_1 subunits: N-type $Ca_v2.2$, P/Q-type $Ca_v2.1$, R-type $Ca_v2.3$ and L-type $Ca_v1.2$ channels in BHK cells. The most prominent RIM1 effect on VDCC currents was observed on inactivation parameters. Inactivation was markedly decelerated in N-, P/Q-, R- and L-type currents (**Fig. 4a**,**b**). The same set of VDCC types also showed a significant depolarizing shift in the voltage dependence of inactivation (**Fig. 4c**,**d**; see **Supplementary Table 1** for statistical significance). In P/Q-type currents (with β_{4b}), RIM1 shifted the half-inactivation potential ($V_{0.5}$) by +24.6 mV, eliciting an inactivation curve with a component that was susceptible to inactivation induced at high voltages ($V_{0.5}$ (vector) = –45.9 mV, $V_{0.5}$ (RIM1) = –21.3 mV) and a component that was non-inactivating. In N- and R-type currents, RIM1 provoked a switch in the major phase of biphasic inactivation curves from low voltage induced ($V_{0.5}$ and ratio: –64.5 mV and 0.91 for N, and –78.2 mV and 0.91 for R) to high voltage induced ($V_{0.5}$ and ratio: –20.8 mV and 0.61 for N, and –27.9 mV and 0.53 for R). The L-type inactivation curve remained monophasic; however, the non-inactivating component was significantly augmented by RIM1 (from 0.07 to 0.25; $P < 0.05$). In P/Q-type, similar RIM1 effects on inactivation were observed with all other β subunits tested (**Fig. 4a**,**c** and **Supplementary Table 2** online). Furthermore, the C-terminal truncated mutants $RIM1_{1079–1463}$ and $RIM1_{1258–1463}$, but not $RIM1_{1079–1257}$, successfully slowed P/Q-type

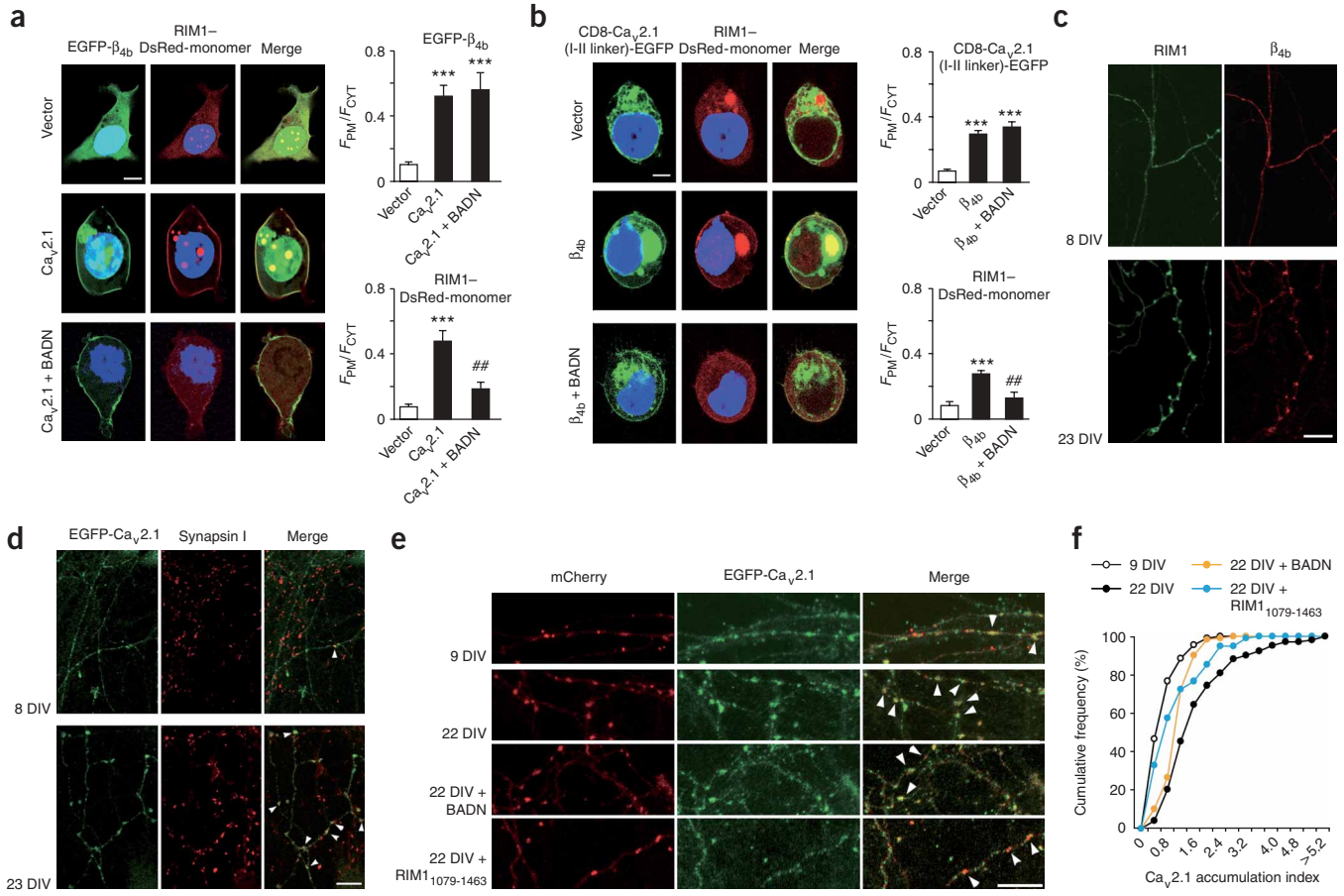

Figure 3 RIM1 clusters with the VDCC subunits near presynaptic termini in cultured hippocampal neurons. (**a**) $Ca_v2.1$ elicited plasma membrane (PM) colocalization of β_{4b} with RIM1. BADN disrupted colocalization. Left, confocal imaging of HEK293 cells expressing EGFP-β_{4b} and RIM1–DsRed-monomer with vector, $Ca_v2.1$ or $Ca_v2.1$ plus BADN. Scale bar, 5 μm. Nuclei were stained with Hoechst 33342. Right, subcellular location of EGFP-β_{4b} or RIM1–DsRed-monomer in 1-μm widths of the plasma membrane region and in the cytosolic area (CYT) ($n = 5$). $^{***}P < 0.001$ versus vector. $^{\#\#}P < 0.01$ versus $Ca_v2.1$. (**b**) β_{4b} elicited plasma membrane colocalization of $Ca_v2.1$(I-II linker) and RIM1. BADN disrupted colocalization. Left, confocal imaging of HEK293 cells expressing CD8-$Ca_v2.1$(I-II linker)-EGFP and RIM1–DsRed-monomer with vector, β_{4b} or β_{4b} and BADN. Right, subcellular location of CD8-$Ca_v2.1$(I-II linker)-EGFP or RIM1–DsRed-monomer ($n = 5$). $^{***}P < 0.001$ versus vector. $^{\#\#}P < 0.01$ versus β_{4b}. (**c**) Immunolocalization of tagged RIM1 and β_{4b} in cultured hippocampal neurons. Clustering of RIM1 and β_{4b} was undetected at 8 DIV, but was present at a substantially later stage at 23 DIV. Scale bar, 10 μm. (**d**) Late clustering of EGFP-$Ca_v2.1$ (arrowheads) in hippocampal neurons. Synapsin I–positive puncta were already abundant at 8 DIV, while $Ca_v2.1$ distribution was still diffuse. Like RIM1 and β_{4b}, $Ca_v2.1$ clustered much later on. (**e**,**f**) Accumulation of EGFP-$Ca_v2.1$ (arrowheads) in presynaptic varicosities was achieved between 9 and 22 DIV. This maturation process was impaired by $RIM1_{1079–1463}$ or BADN, suggesting that the local VDCC concentration at presynaptic active zones is influenced by RIM1–β-subunit interaction during a postsynaptogenic maturation period.

(with β_{1a}) current inactivation (**Fig. 4a,c** and **Supplementary Table 3** online).

After RIM1 coexpression, single-channel P/Q-type currents clearly showed a prolongation of the mean time between first channel opening and last closing within a trace during 750-ms depolarizations to +20 mV without substantial changes in amplitude (0.59 pA, **Fig. 4e**). This observation corresponds well with the whole-cell data and suggests that RIM1 predominantly stabilizes the non-inactivating

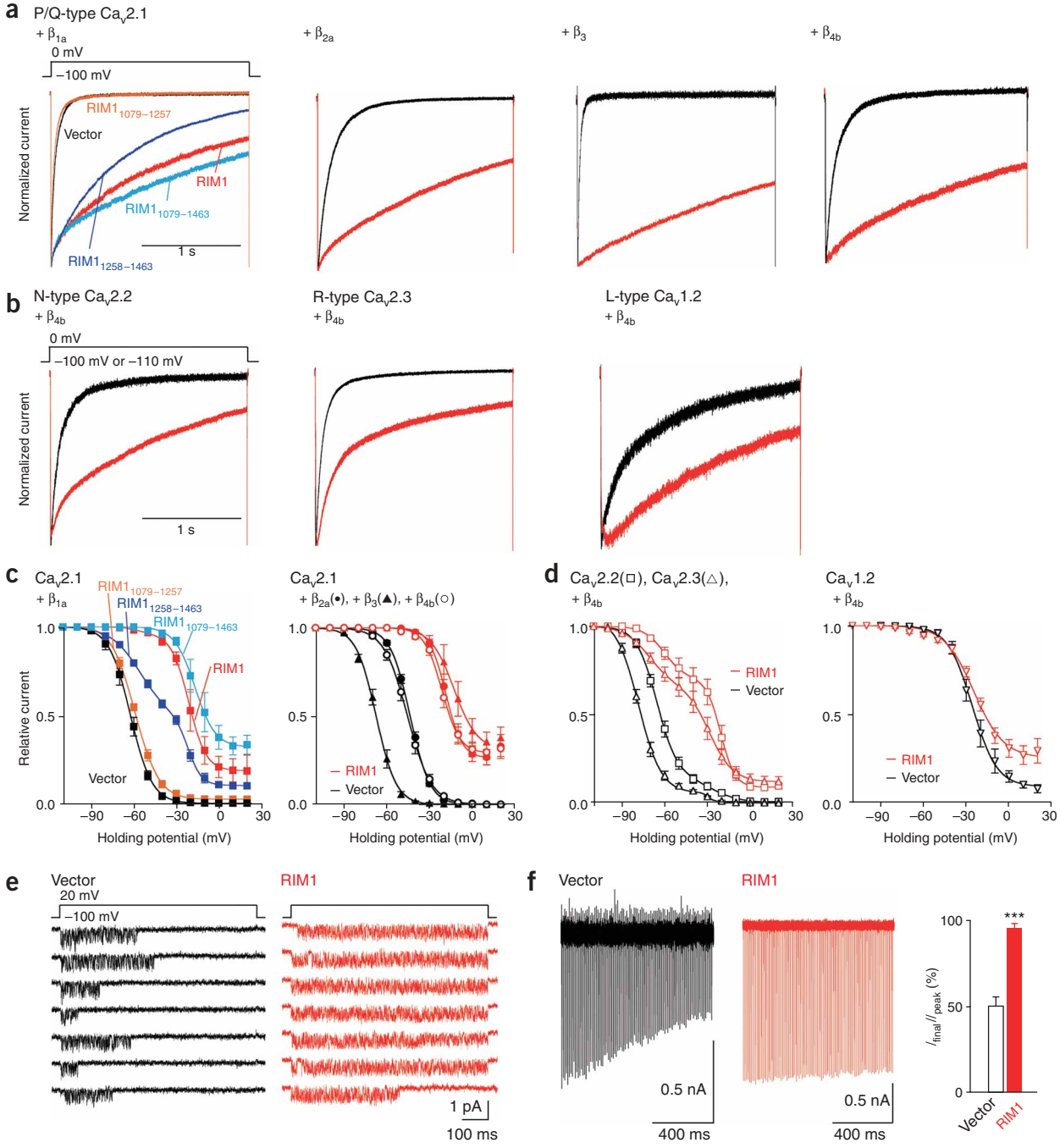

Figure 4 Effects of RIM1 on the inactivation properties of recombinant neuronal VDCCs. (**a**) Inactivation of P/Q-type $Ca_v2.1$ currents in BHK cells. The peak amplitudes before and after coexpression of RIM1 constructs were normalized for Ba^{2+} currents elicited by 2-s pulses to 0 mV from a holding potential (V_h) of –100 mV. (**b**) Inactivation of N-type $Ca_v2.2$, R-type $Ca_v2.3$ or L-type $Ca_v1.2$ currents (with β_{4b}). The V_h was –100 mV ($Ca_v2.2$, $Ca_v1.2$) or –110 mV ($Ca_v2.3$). (**c**) Left, inactivation curves for $Ca_v2.1$ (with β_{1a}). Right, inactivation curves for $Ca_v2.1$ in BHK cells expressing α_2/δ and different β subunits. See **Supplementary Tables 2** and **3** for statistical significance of the differences. (**d**) Inactivation curves for $Ca_v2.2$, $Ca_v2.3$ (left), or $Ca_v1.2$ (right) (with β_{4b}). See **Supplementary Table 1** for statistical significance of the differences. (**e**) RIM1 prolonged the time between first channel opening and last closing within a single-channel trace of $Ca_v2.1$ (with β_{4b}). Seven consecutive unitary traces are shown. The mean values for the time of each trace were 184.2 ± 33.3 ms ($n = 117$ traces) for vector and 502.8 ± 33.3 ms ($n = 101$) for RIM1. The time for traces without opening was counted as 0 ms. (**f**) Left, $Ca_v2.1$ currents (with β_{1a}) induced by 100-Hz action potential trains for 1 s. Right, percentage of currents in response to the last stimulus compared with the peak current ($n = 6$ for vector and $n = 4$ for RIM1). $^{***}P < 0.001$.

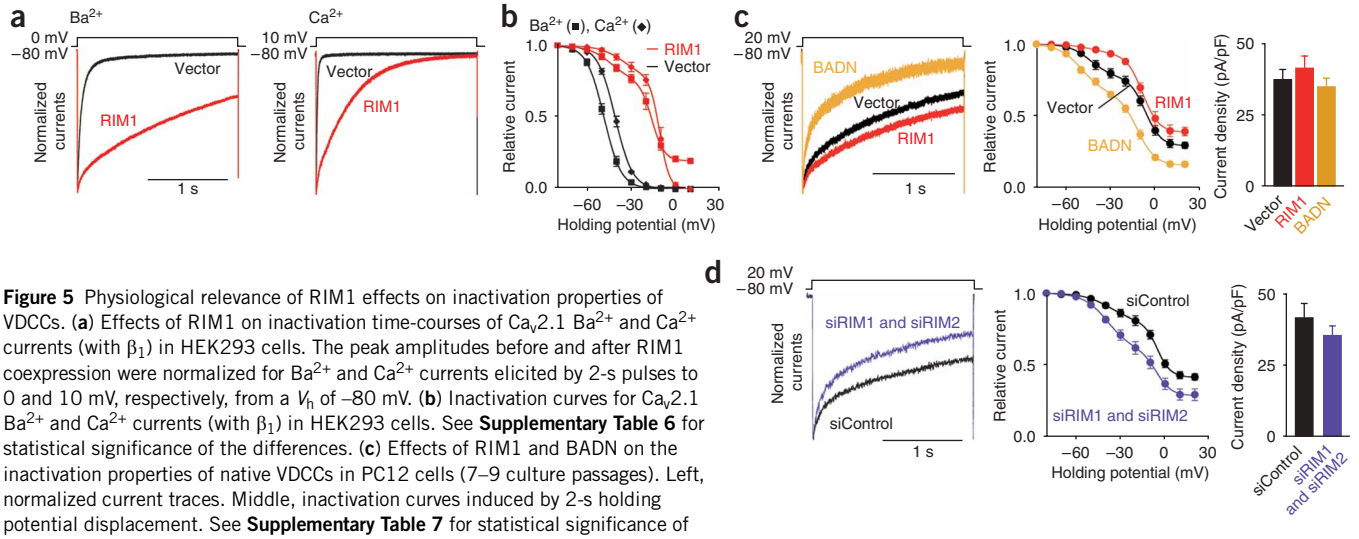

Figure 5 Physiological relevance of RIM1 effects on inactivation properties of VDCCs. (**a**) Effects of RIM1 on inactivation time-courses of $Ca_v2.1$ Ba^{2+} and Ca^{2+} currents (with β_1) in HEK293 cells. The peak amplitudes before and after RIM1 coexpression were normalized for Ba^{2+} and Ca^{2+} currents elicited by 2-s pulses to 0 and 10 mV, respectively, from a V_h of –80 mV. (**b**) Inactivation curves for $Ca_v2.1$ Ba^{2+} and Ca^{2+} currents (with β_1) in HEK293 cells. See **Supplementary Table 6** for statistical significance of the differences. (**c**) Effects of RIM1 and BADN on the inactivation properties of native VDCCs in PC12 cells (7–9 culture passages). Left, normalized current traces. Middle, inactivation curves induced by 2-s holding potential displacement. See **Supplementary Table 7** for statistical significance of the differences. Right, comparison of current densities at 10 mV ($n = 18$, 15 and 9 cells for vector, RIM1 and BADN, respectively). (**d**) Acceleration of inactivation by application of siRNAs specific for RIM1 and RIM2 (siRIM1 and siRIM2) in VDCC currents recorded from PC12 cells (2–3 culture passages). Left, normalized current traces. Middle, inactivation curves. See **Supplementary Table 7** for statistical significance of the differences. Right, comparison of current densities at 10 mV ($n = 6$ and 8 cells, for siControl, and siRIM1 and siRIM2, respectively).

mode[35]. Currents evoked by trains of action potential waveforms, a more physiological voltage-clamp protocol used to determine closed-state inactivation[36], further support the existence of a profound suppression of voltage-dependent inactivation by RIM1 (**Fig. 4f**).

The observed effect of RIM1 on VDCC inactivation is attributable to its association with the β subunit, as replacement of β_4 with the C-terminal truncation construct β_4-GK[37], which directly interacts with α_1 but lacks the ability to bind RIM1, did not substantially affect inactivation of N-type currents (**Supplementary Fig. 5** and **Supplementary Table 4** online). In addition, BADN significantly diminished the RIM1 effect on P/Q channel inactivation (**Supplementary Fig. 5** and **Supplementary Table 5** online for statistical significance). When 5 mM Ca^{2+} was used as a physiological charge carrier capable of inducing both Ca^{2+}-dependent and voltage-dependent inactivation[38], RIM1 still exerted prominent suppressive effects on inactivation in P/Q-type currents expressed in HEK293 cells (**Fig. 5a**,**b** and **Supplementary Table 6** online). Notably, in rat PC12 neuroendocrine cells, BADN or application of siRNAs that specifically suppress RIM1 and RIM2 expression accelerated inactivation and shifted the inactivation curve toward the hyperpolarizing direction (**Fig. 5c**,**d** and **Supplementary Table 7** online). This supports a physiologically significant role for RIM-mediated VDCC modulation via the β subunit. Notably, as observed in RIM1-expressing cells, voltage-dependent inactivation of presynaptic VDCC currents at membrane potentials ≥–40 mV has been previously demonstrated[39]. Thus, RIM1 exerts strong suppressive effects on the kinetics and voltage dependence of inactivation of VDCC currents.

RIM1's effects on other functional current parameters such as voltage dependence of activation, activation kinetics and current densities at different voltages in current-voltage relationships differentiate VDCCs into two different groups (**Fig. 6** and **Supplementary Table 1**). In β_{4b}-expressing BHK cells, the current densities of N- and P/Q-type currents were significantly augmented by RIM1, whereas those of R- and L-type currents were unaffected by RIM1 (**Fig. 6c**,**d**; and see **Supplementary Table 1** for statistical significance). In P/Q-type, $RIM1_{1079–1463}$, which binds β, was sufficient to enhance current density (**Fig. 6c**). By contrast, activation speeds were significantly reduced and activation curves were shifted toward positive potentials by RIM1 in R- and L-types, but not in N- and P/Q-types (**Fig. 6a**,**b**; and see **Supplementary Table 1** for statistical significance). Replacement of β_{4b} with other β isoforms abolished the augmentation of P/Q-type current densities by RIM1 (**Supplementary Fig. 6** online), but slowed the activation speed of P/Q-type by RIM1 (**Fig. 6b**). The RIM1 positive shift in activation curve was also elicited by β_{2a} in P/Q-type (**Supplementary Fig. 6**). Thus, N- and P/Q-type currents responded differently to RIM1 in terms of activation parameters and current densities than did R- and L-type currents, perhaps reflecting different subcellular localizations or functions of these channel subsets.

RIM1-β binding anchors neurotransmitter vesicles to VDCCs

We directly observed vesicles docked to the plasma membrane using evanescent wave microscopy, which illuminates only the subcellular area from the surface to a depth of less than 100 nm by total internal reflection fluorescence (TIRF). Dense-core vesicles were identified by a fusion protein of neuropeptide Y (NPY) and the fluorescent protein Venus in PC12 cells. The overlapping distribution of NPY-Venus, VAMP–DsRed-monomer and RIM1–DsRed-monomer indicated that transmitter-filled synaptic vesicles can be identified using the fluorescent signals of NPY-Venus (**Fig. 7a**). The codistribution is likely to be specific for RIM1, as caveolin-1–enhanced green fluorescent protein (EGFP) did not colocalize with VAMP–DsRed-monomer. The number of docked vesicles was increased significantly by expression of the full-length RIM1 ($P < 0.001$), whereas it was unaffected by $RIM1_{400–1078}$ or by $RIM1_{11–399}$, which forms a ternary complex with Rab3 and Munc13 via a Zn^{2+} finger critical for neurotransmitter release[40] (**Fig. 7b**,**c**). BADN, as well as $RIM1_{1079–1463}$, significantly attenuated the number of docked vesicles ($P < 0.001$ for BADN, $P < 0.05$ for $RIM1_{1079–1463}$). These inhibitory effects of BADN and $RIM1_{1079–1463}$ on vesicle docking most likely occur by quenching endogenous full-length RIMs and by saturating RIM1 interaction sites on VDCC β subunits, respectively. The BADN effect is not due to a reduction in the densities of VDCCs in PC12 cells, as BADN did not substantially affect current densities (**Fig. 5c**). Thus, the 'full-length' structure is probably essential for RIM1 to anchor neurotransmitter vesicles to VDCCs.

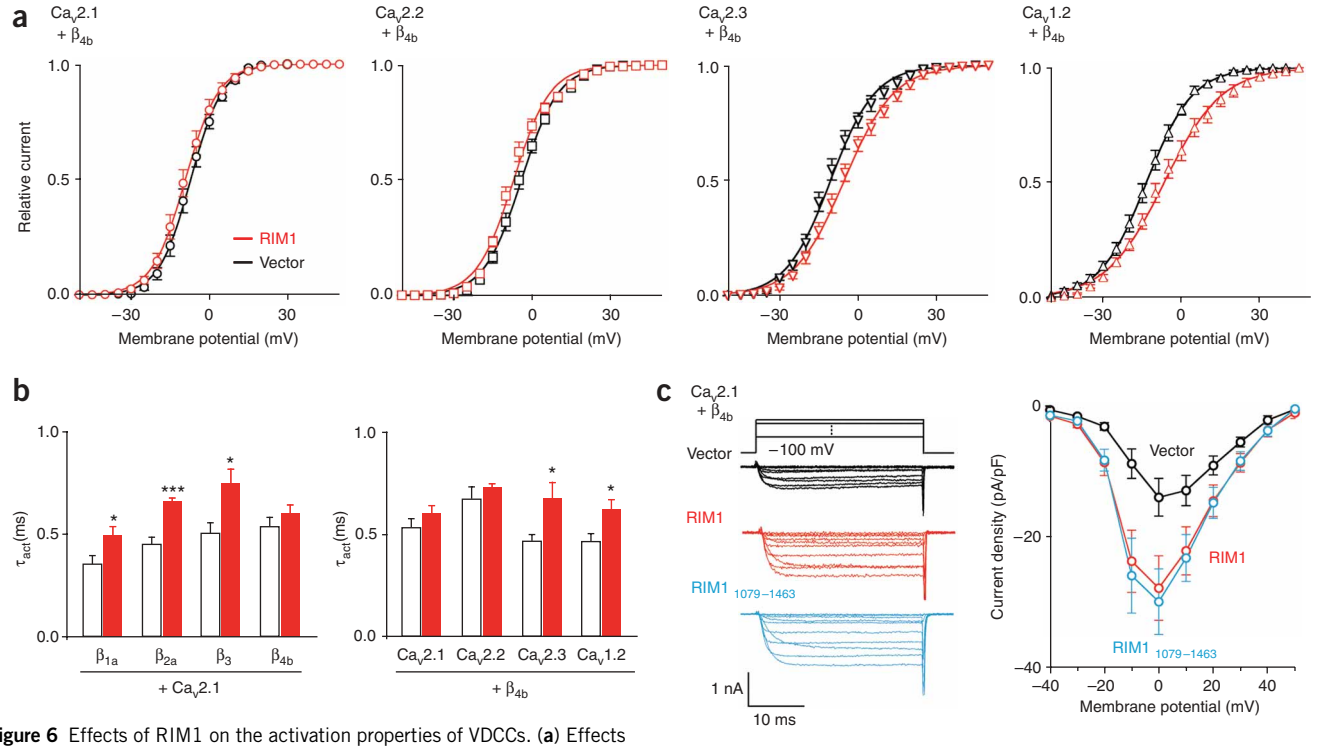

Figure 6 Effects of RIM1 on the activation properties of VDCCs. (**a**) Effects of RIM1 on activation curves of Ca_v currents (with β_{4b}) elicited in BHK cells. Tail currents elicited by repolarization to –60 mV after 5-ms test pulse from –50 to 50 mV were used to determine activation curves. See **Supplementary Table 1** for statistical significance of the differences. (**b**) Left, effects on activation speed of $Ca_v2.1$ channels containing various β subunits. Time constants were obtained by fitting the activation phase of currents elicited by 5-ms test pulse to 20 mV with a single exponential function. Right, effects of RIM1 on activation speed of Ca_v currents at 20 mV in various VDCC types. $^*P < 0.05$ and $^{***}P < 0.001$. (**c**) Effects of RIM1 proteins on P/Q-type $Ca_v2.1$. Left, representative traces for Ba^{2+} currents (with β_{4b}) on application of test pluses from –40 mV to 50 mV with 10-mV increments. Right, current density-voltage (*I-V*) relationships of $Ca_v2.1$. The V_h is –100 mV. See **Supplementary Table 2** for statistical significance of the differences. (**d**) *I-V* relationships of $Ca_v2.2$ (left) and $Ca_v2.3$ or $Ca_v1.2$ (right) (with β_{4b}). The V_h is –100 mV ($Ca_v2.2$, $Ca_v1.2$) or –110 mV ($Ca_v2.3$). See **Supplementary Table 1** for statistical significance of the differences.

RIM1-β interaction enhances neurotransmitter release

We studied the physiological relevance of RIM1 interactions with the VDCC complex by assessing neurotransmitter release from PC12 cells in which diverse high voltage–activated VDCC types have been precisely characterized[35,41] (**Supplementary Fig. 7** online). We transfected PC12 cells with RIM1 construct cDNAs along with *Chat* (encoding choline acetyltransferase), which synthesizes acetylcholine (ACh) for synaptic vesicles[42]. ACh release, triggered by Ca^{2+} influx in response to high-K^+ (elevation of extracellular K^+ concentration from 5.9 mM to 51.1 mM) membrane depolarization, was significantly potentiated by full-length RIM1 (**Fig. 8a** and **Supplementary Fig. 7**, $P < 0.001$). ACh release was also enhanced by the Rab3-interacting N-terminal $RIM1_{11–399}$ and by the C-terminal $RIM1_{1079–1463}$ that maintains VDCC currents, but not by the middle $RIM1_{400–1078}$. In contrast, BADN significantly suppressed ACh release ($P < 0.001$). In cultured cerebellar neurons, similar suppression by BADN and potentiation by the full-length RIM1 were observed for high K^+–induced glutamate release (**Fig. 8b**). The results suggest that RIM1 potentiates neurotransmitter release through its interaction with VDCC β in neuronal and neuron-like cells.

DISCUSSION

The present investigation reveals a previously unknown physical association between the presynaptic active zone proteins RIM1 and VDCC β subunits. The results of yeast two-hybrid assays, *in vitro* binding assays and coimmunoprecipitation experiments have identified a RIM1-VDCC complex formed by direct interaction of the β subunit with the α_1 subunit AID region and the RIM C terminus (residues 1079–1463) (**Fig. 1**). The identification of native RIM1-VDCC complexes in brain (**Fig. 2**), the colocalization of RIM1 with VDCC subunits at the plasma membrane and the presynapse, and the disruption of such localization and complex formation by BADN (**Fig. 3**) support a physiological role for the RIM1-β association. Further biochemical and functional analyses (**Figs. 1** and **4**) suggest that $RIM1_{1079–1257}$ and $RIM1_{1258–1463}$ are the primary β subunit binding site and modulatory region, respectively, in the RIM1 protein. Although our experiments showed that RIM1 and β_4 interacted, the RIM1 in wild-type brains was indistinguishable from that found in the brains of lethargic mice by sucrose gradient profile (**Fig. 2a,d**). It has been previously reported that the immunolocalization of $Ca_v2.1$ and $Ca_v2.2$ in the brain and the properties of P-type currents in Purkinje

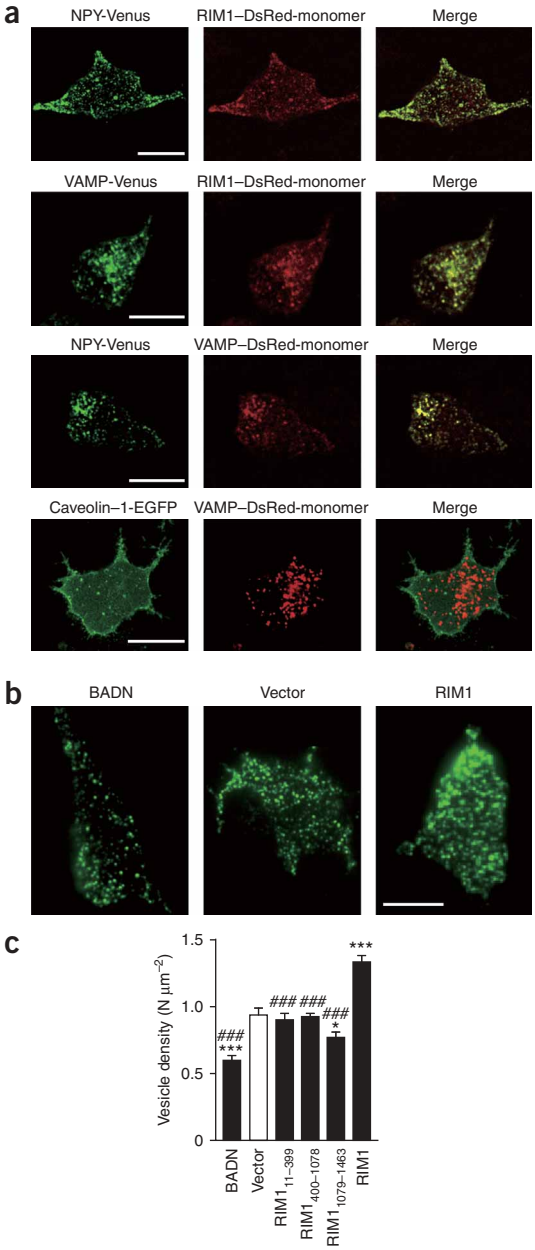

Figure 7 RIM1 and β subunits associate to anchor neurotransmitter vesicles to VDCCs at the plasma membrane. (**a**) NPY-containing secretory vesicles were colocalized with RIM1 and VAMP that was not colocalized with caveolin-1 in PC12 cells. NPY-Venus and RIM1–DsRed-monomer, VAMP-Venus and RIM1–DsRed-monomer, NPY-Venus and VAMP–DsRed-monomer, or caveolin-1–EGFP and VAMP–DsRed-monomer were coexpressed in PC12 cells and live images of the cells were obtained by confocal microscopy. Scale bar, 10 µm. (**b**,**c**) Effects of RIM1 constructs and BADN on the density of docked vesicles. Typical TIRF images of plasma membrane–docked vesicles containing NPY-Venus are shown in **b**. Left, BADN-cotransfected PC12 cell. Middle, vector-cotransfected PC12 cell. Right, RIM1-cotransfected PC12 cell. Scale bar, 10 µm. In **c**, the vesicle density was determined by counting the vesicles in each image ($n = 20$ cells in each). $^{*}P < 0.05$, $^{***}P < 0.001$ versus vector. $^{\#\#\#}P < 0.001$ versus RIM1.

neurons are indistinguishable between wild-type and lethargic mice[32]. This has been attributed to the rescue of β_4 deficiency by the remaining subunits, β_1, β_2 and β_3. We expect a similar compensatory mechanism may also occur in the RIM1-β interaction in lethargic mice. Therefore, the β_4 isoform is unlikely to exclusively mediate the RIM1-VDCC association in the brain.

The RIM1-β association enables RIM1 to have a dual physiological function in neurotransmitter release: sustaining Ca^{2+} influx through the functional regulation of VDCCs and anchoring vesicles to VDCCs (**Supplementary Fig. 8** online). Among the functional parameters of VDCCs, those that are related to voltage-dependent inactivation are most prominently modified by RIM1 through the β interaction (**Fig. 4**). The inactivation kinetics are markedly decelerated, resulting in the predominance of high-voltage inactivation and an inactivation-resistant current component in the 2-s prepulse protocol. The similarly modulated inactivation properties of P/Q-type VDCCs by RIM2α, RIM3γ or RIM4γ (unpublished data), which all carry the C_2B domain, suggest that this function is a common feature for the RIM family[5]. Suppression by BADN of the RIM1-mediated inactivation in both the recombinant (**Supplementary Fig. 5**) and native VDCCs (**Fig. 5c**) provides evidence that RIM1 exerts observed effects through the RIM1-β association. This is supported by our finding that β_4-GK, which binds to α_1 (ref. 37) but not to RIM1, did not mediate RIM1 effects on N-type channels (**Supplementary Fig. 5**). Although the detailed molecular mechanisms underlying inactivation have yet to be determined, previous mapping of the molecular determinants for voltage-dependent inactivation kinetics[43] suggest that RIM1-β complexes bound to the I-II linker AID further act on adjacent segment S6 of repeat I to hinder its conformational transition to the inactivated state. Alternatively, RIM1 may immobilize the β subunit and the process of inactivation by slowing the movement of the I-II loop[44,45]. When voltage-dependent inactivation is thus suppressed, the responses of Ca^{2+} sensors such as synaptotagmins to Ca^{2+} influx may be potentiated at depolarizing membrane potentials that induce voltage-dependent inactivation when RIM1 is absent. Because RIM1 virtually abolished VDCC inactivation that was elicited by a train of action potential waveforms (**Fig. 4f**), certain forms of synaptic depression via closed-state inactivation[36] may be minimized by RIM1 at presynaptic active zones. The impact of the RIM1-β association on delaying VDCC inactivation may explain recent findings with the RIM1α knockout mouse showing that RIM1 is important for the late-stage asynchronous neurotransmitter release, whereas synaptotagmin I is involved in the earlier synchronous release[12]. With P/Q- and N-type channels, the RIM1-β association significantly affected channel activity as well; current densities were nearly doubled by RIM (**Fig. 6c**). Thus, RIM1 can maintain and enhance depolarization-induced Ca^{2+} influx to support neurotransmitter release at presynaptic active zones.

Regarding the role of RIM1 in vesicle anchoring to VDCC at the plasma membrane, full-length RIM1 is required to mediate vesicle anchoring, in contrast to the RIM1 suppression of VDCC inactivation, which requires only the RIM1 C terminus. Taking into consideration the direct RIM1-Rab3 association and the regulation of tethering and/or priming of synaptic vesicles by Rab3 (ref. 40), it is likely that simultaneous interactions of RIM1 with vesicle-associated Rab3 and Munc13 via the N-terminal Zn^{2+}-finger domain and with the VDCC β subunit via the C-terminal C_2B domain underlie, at least in part, the maintenance of the close proximity of VDCCs to vesicles, thereby regulating the dynamic properties of synaptic transmission[3]. Supporting this idea, BADN and $RIM1_{1079–1463}$ significantly suppressed vesicle docking in PC12 cells (**Fig. 7c**). In our experiments, however, RIM1 and β subunit targeting to the presynaptic site was observed only after early synapse formation (**Fig. 3**). It is possible that the interaction of Mint and CASK with VDCC α_1 subunits via their C termini[22,23] may

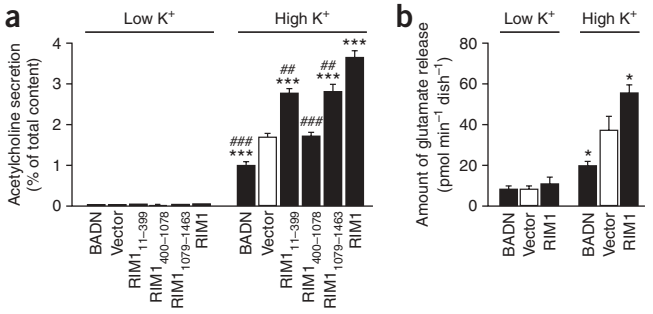

Figure 8 The RIM1-β association enhances neurotransmitter release in PC12 cells and cultured cerebellar neurons. (**a**) Effects of RIM1 constructs and BADN on depolarization-dependent release of ACh from ChAT-cotransfected PC12 cells. Three days after transfection, PC12 cells were incubated for 30 s with low-K^+ solution (5.9 mM K^+) at 37 °C. The release of ACh during this period was considered to be basal release. To measure ACh release, the cells were then incubated for 30 s with a high-K^+ solution (51.1 mM K^+). The amount of secreted ACh was determined as a percentage of the cellular content for each dish. $^{***}P < 0.001$ versus vector. $^{\#\#}P < 0.01$, $^{\#\#\#}P < 0.001$ versus RIM1. (**b**) Effects of RIM1 and BADN on depolarization-dependent release of glutamate from cultured cerebellar neurons. Twenty-four hours after the introduction of cDNAs, cerebellar neurons (9–11 DIV) were incubated for 1 min with the low-K^+ solution (5.9 mM K^+) at 37 °C. The release of glutamate during this period was considered to be basal release. To measure glutamate release, the cells were then incubated for 1 min with a high-K^+ solution (51.1 mM K^+). $^*P < 0.05$.

also direct channel targeting in parallel of, or before, RIM1–β subunit complex formation. Notably, our observation is consistent with a previous report[46] stating that the loss of the RIM homolog UNC10 caused a reduction in membrane-contacting synaptic vesicles within 30 nm of the dense projection at *Caenorhabditis elegans* neuromuscular junctions. Furthermore, in RIM1α-deficient mice, the decay of excitatory postsynaptic currents (EPSCs) during 14-Hz trains of presynaptic stimulation is abolished, whereas the rate at which the readily releasable vesicle pool is refilled is indistinguishable between the wild-type and RIM1α mutant mice[12]. These data suggest that RIM1-mediated vesicles anchoring to VDCCs may enable a rapid depletion of vesicle pools such that the available vesicles are exhausted, leading to EPSC decay. In this scenario, RIM1 knockout would minimize rapid vesicle release, enabling the readily releasable pool to be maintained and thus prevent EPSC decay. More recently, it has been reported that mice deficient in both RIM1α and RIM2α show lethality due to defects in Ca^{2+}-triggered release despite normal presynaptic active zone length and normal spontaneous neurotransmitter release[47]. In combination, these studies support our model (**Supplementary Fig. 8**), predicting a dual function for the RIM1-β interaction in neurotransmitter release by coordinating the molecular constituents and Ca^{2+} signaling in presynaptic active zones.

Previous reports have demonstrated the functional impact of syntaxin, synaptosome-associated protein (SNAP-25) and synaptotagmin on VDCCs through physical association with the 'synprint' region in the II-III linker of α_1-proteins[19–21]. It has been reported[48] that RIM associates with the synprint[10] directly via the C_2A domain, and with the α_1 C-terminal tail indirectly via the RIM-binding protein (RIM-BP) (**Fig. 1a**). However, RIM1 regulation of VDCCs may be independent of the synprint- or RIM-BP–mediated association, because $RIM1_{1079–1463}$, which lacks both the C_2A domain necessary for synprint binding[10] and the PXXP motif for the RIM-BP binding, is still sufficient to inhibit VDCC inactivation (**Fig. 4a,c**). This is supported by our observation that BADN, or replacement of β with β_4-GK, was sufficient to disrupt the RIM1 effects on inactivation (**Supplementary Fig. 5**). Syntaxin and SNAP-25 have been proposed to inhibit VDCC-mediated Ca^{2+} influx via a hyperpolarizing shift of the inactivation curve in the absence of vesicle docking at VDCC sites[19,21], whereas our finding implies enhancement or maintenance of the Ca^{2+} influx via interaction with RIM1 during the docking of vesicles. Notably, previous reports suggest that RIM1 is involved in the modification of the release apparatus at a late stage in the vesicle cycle[9], particularly in the postdocking step[49]. In early phases of vesicle docking, VDCC α_1 interactions with syntaxin and SNAP25 (refs. 19–21) and Mint and CASK[22,23] may be important, eliciting partial resistance to BADN suppression of vesicle docking (**Fig. 7c**). Thus, the α_1 protein associations and the RIM1-β association may be distinct interactions that contribute at different stages of vesicle cycling to controlling the Ca^{2+} supply from the source, namely the VDCC, in addition to regulating the proximity between the Ca^{2+} source VDCC and the target Ca^{2+} sensors at the presynaptic active zone.

METHODS

cDNA expression, cell culture, molecular modeling, recombinant proteins and infection with Sindbis viruses. Methods for cDNA cloning and expression, cell culture, molecular modeling of BADN, preparation of GST fusion proteins and purified β_{4b}-subunit recombinants, and the preparation and infection of Sindbis viruses can be found in the **Supplementary Methods** online.

Yeast two-hybrid screening and β-galactosidase assay. We subcloned rat β_{4b} subunit (GenBank accession number XM_215742) into pGBK-T7 and used it as a bait to screen a mouse brain pACT2 library in the yeast strain AH109 (Clontech). We plated transformants (1.5×10^6) on synthetic medium lacking adenine, histidine, leucine and tryptophan and assayed His^+ colonies for β-galactosidase activity with a filter assay. Of the transformants, 103 were His^+, and 21 of these were also $LacZ^+$. We isolated prey clone no. 2–5, encoding $RIM1_{1079–1463}$ (NM_053270).

***In vitro* binding of the purified proteins, GST-pulldown and coimmunoprecipitation experiments.** RIM1-GST fusion proteins at various concentrations were incubated with 50 pM purified recombinant β_4 subunits for 3 h at 4 °C. Proteins were subjected to western blotting with an antibody for β_4 raised against the peptide ENYHNERARKSRNRLS. The densities of protein signals, obtained using NIH Image (National Institute of Mental Health) under the linear relationship with the applied amount of proteins (**Supplementary Fig. 2**), were normalized to the densities from the maximal binding. For the pulldown assays, the cell lysate was incubated with glutathione-Sepharose beads bound to purified fusion proteins. The proteins were characterized by western blotting with antibody for Myc (Invitrogen). For coimmunoprecipitation, the cell lysate was incubated with anti-FLAG M2 monoclonal antibody (Sigma), and the immunocomplexes were characterized by western blotting with antibody for Myc. For details, see **Supplementary Methods**.

Biochemistry of native neuronal VDCC complexes. VDCC complexes were partially purified from the brains of C57BL/6 or lethargic mice (B6EiC3Sn-*a/A-Cacnb4*^{lh}/J, Jackson Laboratory) as previously reported[25]. KCl washed microsomes (50 mg) were solubilized in buffer I (for buffers, see **Supplementary Table 8** online) and centrifuged at 142,000*g* for 37 min. The supernatant was incubated with heparin-agarose (Sigma); agarose was washed with buffer II and III before elution with buffer IV. After elution, samples were diluted to 150 mM NaCl by addition of buffer V and concentrated using centrifugal filter devices (Millipore). The samples were applied to 5–40% sucrose density gradients (buffer VI) and were centrifuged at 215,000*g* for 90 min. Western blots were performed using antibodies for RIM (BD Biosciences), $Ca_v2.1$ (Alamone), syntaxin (Sigma) and β_4 (described above). Western blot band densities (NIH image) were normalized from four to five independent experiments.

For immunoprecipitation, partially purified neuronal VDCC complexes were incubated with protein A–agarose coupled to antibodies for β_4 or RIM1[4]. Immunoprecipitated proteins were subject to western blotting with

antibodies for RIM or $Ca_v2.1$. To disrupt the physiological association of native RIM1 with VDCC β_4, partially purified VDCC complexes were incubated with 200 nM GST-BADN and GST-$RIM1_{1079–1463}$ for 8 h at 4 °C before immunoprecipitation.

Confocal imaging. At 32 h after transfection, HEK293 cells or PC12 cells were plated on poly-L-lysine–coated glass coverslips. Hoechst 33342 (1 μg ml^{-1}, Dojindo) was added to stain nuclei 56 h after transfection. The imaging was performed in modified Ringer's buffer that contained 130 mM NaCl, 3 mM KCl, 5 mM $CaCl_2$, 1.5 mM $MgCl_2$, 10 mM glucose and 10 mM HEPES (pH 7.4). Fluorescence images were acquired with a confocal laser-scanning microscope (FV500, Olympus). For details, see the **Supplementary Methods**.

TIRF imaging. PC12 cells cotransfected with 1 μg pVenus-N1-NPY and RIM1 expression plasmids at the equal molar quantity (5.0 μg $RIM1_{11–399}$, 5.7 μg $RIM1_{400–1078}$, 5.0 μg $RIM1_{1079–1463}$ or 7.5 μg RIM1) and BADN (10 μg) using OptiFect (Invitrogen) were plated onto poly-L-lysine–coated coverslips. PCR analysis showed that the RIM plasmids were transfected at the equal level (**Supplementary Fig. 7**). The imaging was performed in modified Ringer's buffer. Fluorescence images of NPY-Venus were taken at the single vesicle level using an inverted microscope (IX71, Olympus). Incident light for total internal reflection illumination was introduced from the high numerical objective lens through a single mode optical fiber. Images were captured by a cooled CCD camera (EM-CCD, Hamamatsu Photonics). Area calculations and fluorescent spot counting were performed using Metamorph software (Molecular Devices). The cells showing distribution of vesicles with <10 μm^2 dark circle area that can be placed in between vesicles were selected as cells with uniformly distributed vesicles. The maximal dark circle area in the images from BADN-transfected cells with uniform vesicle distribution was 10 μm^2. For details, see the **Supplementary Methods**.

Immunostaining of cultured hippocampal neurons. Culture and transfection of mouse hippocampal neurons were carried out as described[50]. EGFP-tagged $Ca_v2.1$, Myc-tagged RIM1 and FLAG-tagged β_{4b} were detected with a Zeiss LSM510META confocal microscope using a combination of antibodies: FLAG M2 monoclonal, Myc polyclonal (Cell Signaling) and Alexa488- and Alexa594-conjugated secondary antibodies (Invitrogen). See the **Supplementary Methods** for further quantification procedures.

Current recordings. Whole-cell mode of the patch-clamp technique was carried out at 22–25 °C. An external solution contained 3 mM $BaCl_2$, 155 mM tetraethylammonium chloride (TEA-Cl), 10 mM HEPES and 10 mM glucose for BHK cells, and 10 mM $BaCl_2$, 153 mM TEA-Cl, 10 mM HEPES and 10 mM glucose for PC12 cells (pH 7.4). The pipette solution contained 95 mM CsOH, 95 mM aspartate, 40 mM CsCl, 4 mM $MgCl_2$, 5 mM EGTA, 2 mM disodium ATP, 5 mM HEPES and 8 mM creatine phosphate (pH 7.2). To characterize Ca^{2+}-dependent inactivation, external solutions contained 5 mM $CaCl_2$ or $BaCl_2$, 153 mM TEA-Cl, 10 mM HEPES and 10 mM glucose (pH 7.4). The pipette solution contained 135 mM Cs-$MeSO_3$, 5 mM CsCl, 0.5 mM EGTA, 5 mM $MgCl_2$, 4 mM disodium ATP and 10 mM HEPES (pH 7.2). Single-channel currents were recorded using cell-attached patch mode. The bath solution contained 150 mM KCl, 5 mM HEPES, 0.2 mM EGTA and 10 mM glucose (pH 7.4). The pipette solution contained 110 mM $BaCl_2$ and 10 mM HEPES (pH 7.4). 750-ms voltage steps were given every 5 s from a V_h of –100 mV. Details of current recordings and analyses, including voltage dependence of inactivation and activation and action potential train, are described in the **Supplementary Methods**.

Suppression of the action of endogenous RIMs using siRNAs and BADN in PC12 cells. The sense siRNA sequences 5′-AAGAATGGACCACAAATGCTT-3′ and 5′-AAGGTGATTGGATGGTATAAA-3′ for rat RIM1, and 5′-AAGGC CCAGATACTCTTAGAT-3′ and 5′-AAGAACTATCCAACATGGTAA-3′ for rat RIM2, were used. Suppression of RNA expression was confirmed by RT-PCR analyses (**Supplementary Fig. 7**). The cells transfected with 8.0 μg pCI-neo-BADN or 8.0 μg pCI-neo-RIM1 were subjected to current recordings 72–96 h after transfection. For details, see the **Supplementary Methods**.

Release assay and RNA analysis in PC12 cells. RNA expression of the α_1 subunits, β subunits, RIM1 or RIM2 in PC12 cells was determined by RT-PCR (**Supplementary Fig. 7**; see **Supplementary Table 9** online for primers). ACh secretion experiments were carried out as previously reported with slight modifications[42]. PC12 cells were plated in poly-D-lysine–coated 35-mm dishes (BD Bioscience) with 5×10^5 cells per dish. Cells were cotransfected with 1 μg of pEFmChAT encoding mouse *Chat* cDNA and RIM1 plasmids at equal molar quantity (3.4 μg of $RIM1_{11–399}$, 3.8 μg of $RIM1_{400–1078}$, 3.4 μg of $RIM1_{1079–1463}$ or 5.0 μg of RIM1) and BADN (10 μg) using Lipofectamine 2000 (Invitrogen). ACh secretion experiments were carried out 3 d after transfection. For details, see the **Supplementary Methods**.

Glutamate release assay using cerebellar neuron primary cultures. Cerebellar granular cells were plated on polyethylenimine-coated 35-mm diameter culture dishes (BD Falcon) at a density of 4.5×10^6–5.0×10^6 cells per dish. BADN or RIM1 cDNAs were introduced with Sindbis viruses in cerebellar neurons. At 24 h after infection, high K^+–evoked glutamate release was carried out. For details, see the **Supplementary Methods**.

Statistical analysis. All data accumulated under each condition from at least three independent experiments are expressed as means ± s.e.m. Student's *t*-test, Kolmogorov-Smirnov test or ANOVA followed by Fisher's test were employed.

Note: Supplementary information is available on the Nature Neuroscience website.

ACKNOWLEDGMENTS

We thank A. Miyawaki for NPY-Venus, R.Y. Tsien for mCherry, S. Ozawa for pSinEGdsp vector, H. Hibino, H Atomi and H. Okuno for helpful discussions, K. Yamazaki, K. Ueda, N. Yokoi and Y. Honjo for expert experiments and K. Sugimoto and T. Morii for molecular modeling. This study was supported by research grants from the Ministry of Education, Culture, Sports, Science and Technology of Japan, the Japan Society for the Promotion of Science and the Human Frontier Science Program. K.P.C. is an Investigator of the Howard Hughes Medical Institute.

AUTHOR CONTRIBUTIONS

S.K., M.W., T.M. and Y.U. contributed to the acquisition, analysis and interpretation of data, and drafting of the manuscript. H.B., A.M.B., M.T. and K.P.C. contributed to the analysis and interpretation of data, and drafting of the manuscript. E.M., Y.H., M.N., M.D.W., M.K. and M.I. contributed to the acquisition, analysis and interpretation of data. Y.M. contributed to the analysis and interpretation of data, and drafting and critical review of the manuscript.

COMPETING INTERESTS STATEMENT

The authors declare no competing financial interests.

Published online at http://www.nature.com/natureneuroscience
Reprints and permissions information is available online at http://npg.nature.com/reprintsandpermissions

1. Zhai, R.G. & Bellen, H.J. The architecture of the active zone in the presynaptic nerve terminal. *Physiology (Bethesda)* **19**, 262–270 (2004).
2. Atwood, H.L. Gatekeeper at the synapse. *Science* **312**, 1008–1009 (2006).
3. Neher, E. Vesicle pools and Ca^{2+} microdomains: new tools for understanding their roles in neurotransmitter release. *Neuron* **20**, 389–399 (1998).
4. Wang, Y., Okamoto, M., Schmitz, F., Hofmann, K. & Südhof, T.C. Rim is a putative Rab3 effector in regulating synaptic-vesicle fusion. *Nature* **388**, 593–598 (1997).
5. Wang, Y. & Südhof, T.C. Genomic definition of RIM proteins: evolutionary amplification of a family of synaptic regulatory proteins. *Genomics* **81**, 126–137 (2003).
6. Wang, Y., Sugita, S. & Südhof, T.C. The RIM/NIM family of neuronal C_2 domain proteins. *J. Biol. Chem.* **275**, 20033–20044 (2000).
7. Betz, A. *et al.* Functional interaction of the active zone proteins Munc13-1 and RIM1 in synaptic vesicle priming. *Neuron* **30**, 183–196 (2001).
8. Ohtsuka, T. *et al.* CAST: a novel protein of the cytomatrix at the active zone of synapses that forms a tenary complex with RIM1 and Munc13-1. *J. Cell Biol.* **158**, 577–590 (2002).
9. Schoch, S. *et al.* RIM1α forms a protein scaffold for regulating neurotransmitter release at the active zone. *Nature* **415**, 321–326 (2002).
10. Coppola, T. *et al.* Direct interaction of the Rab3 effector RIM with Ca^{2+} channels, SNAP-25, and synaptotagmin. *J. Biol. Chem.* **276**, 32756–32762 (2001).
11. Castillo, P.E., Schoch, S., Schmitz, F., Südhof, T.C. & Malenka, R.C. RIM1α is required for presynaptic long-term potentiation. *Nature* **415**, 327–330 (2002).
12. Calakos, N., Schoch, S., Südhof, T.C. & Malenka, R.C. Multiple roles for the active zone protein RIM1α in late stages of neurotransmitter release. *Neuron* **42**, 889–896 (2004).

13. Tsien, R.W., Ellinor, P.T. & Horne, W.A. Molecular diversity of voltage-dependent Ca^{2+} channels. *Trends Pharmacol. Sci.* **12**, 349–354 (1991).
14. Takahashi, T. & Momiyama, A. Different types of calcium channels mediate central synaptic transmission. *Nature* **366**, 156–158 (1993).
15. Wheeler, D.B., Randell, A. & Tsien, R.W. Roles of N-type and Q-type Ca^{2+} channels in supporting hippocampal synaptic transmission. *Science* **264**, 107–111 (1994).
16. Catterall, W.A. Structure and function of neuronal Ca^{2+} channels and their role in neurotransmitter release. *Cell Calcium* **24**, 307–323 (1998).
17. Ertel, E.A. *et al.* Nomenclature of voltage-gated calcium channels. *Neuron* **25**, 533–535 (2000).
18. Sheng, Z-H., Rettig, J., Takahashi, M. & Catterall, W.A. Identification of a syntaxin-binding site of N-type calcium channels. *Neuron* **13**, 1303–1313 (1994).
19. Bezprozvanny, I., Scheller, R.H. & Tsien, R.W. Functional impact of syntaxin on gating of N-type and Q-type calcium channels. *Nature* **378**, 623–626 (1995).
20. Zhong, H., Yokoyama, C.T., Scheuer, T. & Catterall, W.A. Reciprocal regulation of P/Q-type Ca^{2+} channels by SNAP-25, syntaxin and synaptotagmin. *Nat. Neurosci.* **2**, 939–941 (1999).
21. Spafford, J.D. & Zamponi, G.W. Functional interactions between presynaptic calcium channels and the neurotransmitter release machinery. *Curr. Opin. Neurobiol.* **13**, 308–314 (2003).
22. Maximov, A., Südhof, T.C. & Bezprozvanny, I. Association of neuronal calcium channels with modular adaptor proteins. *J. Biol. Chem.* **274**, 24453–24456 (1999).
23. Maximov, A. & Bezprozvany, I. Synaptic targeting of N-type calcium channels in hippocampal neurons. *J. Neurosci.* **22**, 6939–6952 (2002).
24. Nishimune, H., Sanes, J.R. & Carlson, S.S. A synaptic laminin–calcium channel interaction organizes active zones in motor nerve terminals. *Nature* **432**, 580–587 (2004).
25. Kang, M.G. *et al.* A functional AMPA receptor–calcium channel complex in the postsynaptic membrane. *Proc. Natl. Acad. Sci. USA* **103**, 5561–5566 (2006).
26. Mori, Y. *et al.* Primary structure and functional expression from complementary DNA of a brain calcium channel. *Nature* **350**, 398–402 (1991).
27. Bichet, D. *et al.* The I–II loop of the Ca^{2+} channel α_1 subunit contains an endoplasmic reticulum retention signal antagonized by the β subunit. *Neuron* **25**, 177–190 (2000).
28. Varadi, G., Lory, P., Schultz, D., Varadi, M. & Schwartz, A. Acceleration of activation and inactivation by the β subunit of the skeletal muscle calcium channel. *Nature* **352**, 159–162 (1991).
29. Béguin, P. *et al.* Regulation of Ca^{2+} channel expression at the cell surface by the small G-protein kir/Gem. *Nature* **411**, 701–706 (2001).
30. Hibino, H. *et al.* Direct interaction with a nuclear protein and regulation of gene silencing by a variant of the Ca^{2+} channel β_4 subunit. *Proc. Natl. Acad. Sci. USA* **100**, 307–312 (2003).
31. Vendel, A.C. *et al.* Alternative splicing of the voltage-gated Ca^{2+} channel β_4 subunit creates a uniquely folded N-terminal protein binding domain with cell-specific expression in the cerebellar cortex. *J. Neurosci.* **26**, 2635–2644 (2006).
32. Burgess, D.L. *et al.* β subunit reshuffling modifies N- and P/Q-type Ca^{2+} channel subunit compositions in *lethargic* mouse brain. *Mol. Cell. Neurosci.* **13**, 293–311 (1999).
33. Opatowsky, Y., Chen, C.C., Campbell, K.P. & Hirsch, J.A. Structural analysis of the voltage-dependent calcium channel β–subunit functional core and its complex with the α_1 interaction domain. *Neuron* **42**, 387–399 (2004).
34. Khanna, R., Li, Q., Sun, L., Collins, T.J. & Stanley, E.F. N-type Ca^{2+} channels and RIM scaffold protein covary at the presynaptic transmitter release face, but are components of independent protein complexes. *Neuroscience* **140**, 1201–1208 (2006).
35. Plummer, M.R., Logothetis, D.E. & Hess, P. Elementary properties and pharmacological sensitivities of calcium channels in mammalian peripheral neurons. *Neuron* **2**, 1453–1463 (1989).
36. Patil, P.G., Brody, D.L. & Yue, D.T. Preferential closed-state inactivation of neuronal calcium channels. *Neuron* **20**, 1027–1038 (1998).
37. De Waard, M., Pragnell, M. & Campbell, K.P. Ca^{2+} channel regulation by a conserved β-subunit domain. *Neuron* **13**, 495–503 (1994).
38. DeMaria, C.D., Soong, T.W., Alseikhan, B.A., Alvania, R.S. & Yue, D.T. Calmodulin bifurcates the local Ca^{2+} signal that modulates P/Q-type Ca^{2+} channels. *Nature* **411**, 484–489 (2001).
39. Stanley, E.F. Syntaxin I modulation of presynaptic calcium channel inactivation revealed by botulinum toxin C1. *Eur. J. Neurosci.* **17**, 1303–1305 (2003).
40. Dulubova, I. *et al.* A Munc13/RIM/Rab3 tripartite complex: from priming to plasticity? *EMBO J.* **24**, 2839–2850 (2005).
41. Liu, H. *et al.* Expression and subunit interaction of voltage-dependent Ca^{2+} channels in PC12 cells. *J. Neurosci.* **16**, 7557–7565 (1996).
42. Nishiki, T. *et al.* Comparison of exocytotic mechanisms between acetylcholine- and catecholamine-containing vesicles in rat pheochromocytoma cells. *Biochem. Biophys. Res. Commun.* **239**, 57–62 (1997).
43. Zhang, J.F., Ellinor, P.T., Aldrich, R.W. & Tsien, R.W. Molecular determinants of voltage-dependent inactivation in calcium channels. *Nature* **372**, 97–100 (1994).
44. Stotz, S.C., Hamid, J., Spaetgens, R.L., Jarvis, S.E. & Zamponi, G.W. Fast inactivation of voltage-dependent calcium channels. *J. Biol. Chem.* **275**, 24575–24582 (2000).
45. Geib, S. *et al.* The interaction between the I–II loop and the III–IV loop of $Ca_v2.1$ contributes to voltage-dependent inactivation in a β-dependent manner. *J. Biol. Chem.* **277**, 10003–10013 (2002).
46. Weimer, R.M. *et al.* UNC-13 and UNC-10/Rim localize synaptic vesicles to specific membrane domains. *J. Neurosci.* **26**, 8040–8047 (2006).
47. Schoch, S. *et al.* Redundant functions of RIM1α and RIM2α in Ca^{2+}-triggered neurotransmitter release. *EMBO J.* **25**, 5852–5863 (2006).
48. Hibino, H. *et al.* RIM-binding proteins (RBPs) couple Rab3-interacting molecules (RIMs) to voltage-gated Ca^{2+} channels. *Neuron* **34**, 411–423 (2002).
49. Koushika, S.P. *et al.* A post-docking role for active zone protein Rim. *Nat. Neurosci.* **4**, 997–1005 (2001).
50. Nonaka, M., Doi, T., Fujiyoshi, Y., Takemoto-Kimura, S. & Bito, H. Essential contribution of the ligand-binding βB/βC loop of PDZ1 and PDZ2 in the regulation of postsynaptic clustering, scaffolding and localization of postsynaptic density–95. *J. Neurosci.* **26**, 763–774 (2006).